1

Introduction

1.1 Introduction

The year twenty-twenty (2020) has witnessed an extraordinarily turbulent year for the global energy system. COVID-19 has adversely affected the lives and livelihoods of countries around the world. This pandemic has caused more disruption to the energy sector than any other event and the impact of this crisis will be felt for years to come [1]. Moreover, the increase of globalisation and thirst for energy has increased the total energy consumption on the planet dramatically. The energy consumption of the world has increased by nearly 12% to 18.3 terawatt year (TWyr) per annum in 2014 and is expected to exceed 27 TWyr per annum by 2050 [2]. However, India is the third-largest energy-consuming country and is set to experience the largest increase in energy demand by an average of 2.6% annually through 2030 [3].

Until now, the majority of energy generation (~ 80%) is delivered by burning coal, natural gas and oil. However, fossil fuel (coal and natural gas) has certain difficulties, including its exhaustible nature and the negative impact on the environment by combustion of fossil fuels. Burning of fossil fuels emits carbon dioxide (CO_2) as an unavoidable by-product which is solely responsible for rising global temperature and climate change, and the continuation of this will cause global warming, depletion of the ozone layer and rise of sea level [4]. Therefore, there is an urgent need to develop alternative solutions to these and to rely more and more on clean energy i.e. natural sources of energy, like solar, wind, geothermal, etc. [5]. Solar energy is one of the most abundant source of clean and renewable energy which is available in plentiful

amount for free (**Figure 1.1)**. Energy sources such as wind, geothermal and hydrothermal require cost intensive equipment and infrastructure. On the other hand, solar energy is abundant and can be utilized at very low cost without harming the environment.

Solar rays hitting the earth everyday consist of photons carrying a huge amount of energy. **Figure 1.2** depicted the amount of solar energy flux received by various parts of the earth depends on the latitude of the geographical area [6]. The countries such as US, Australia, Africa and India are subjected to an annual average solar irradiation exceeding 1600 kWh/m^2. Utilizing only a fraction of this vast available solar energy would power the whole planet. Considering the fact that on average every square meter of earth's surface receives 164 watts of solar energy, which can power the world just by covering only one percent of the Sahara desert with solar panels [7]. One of the most promising ways of utilizing solar energy is photovoltaic technology (PV) which converts incoming solar radiation (photons) directly into usable electrical power via PV effect or photochemical reactions [8]. It is believed that PV can be an option for generation of energy without emitting toxic substance and greenhouse gases [9].

"It may mark the beginning of a new era, leading eventually to the realization of one of mankind's most cherished dreams-the harnessing of almost limitless energy of the sun for the uses of civilization" headlines from The New York Times published on April 26, 1954, highlights the bright future of the solar energy after the development of a solar battery which converts the useful amount of sun radiation directly and efficiently into electricity by the Bell Telephone Laboratories [10].

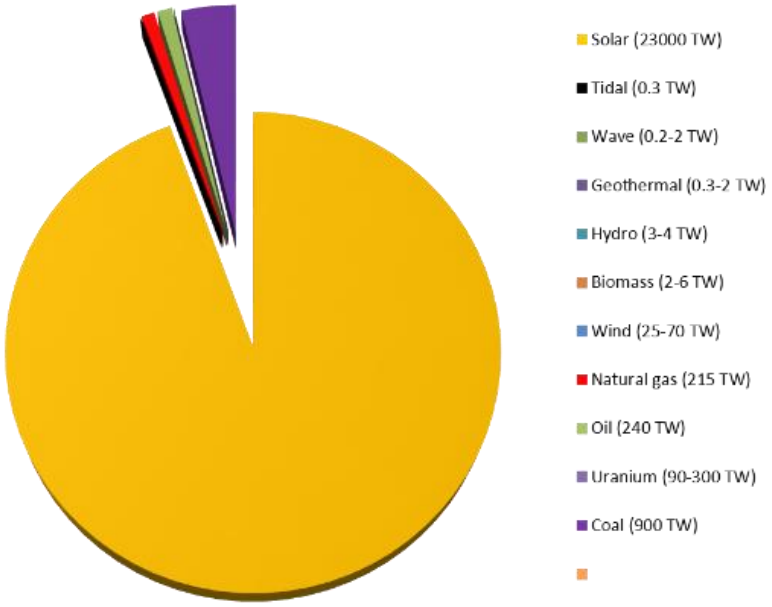

Figure 1.1 Worldwide energy source distribution (Tera Watt). Adapted from [3]

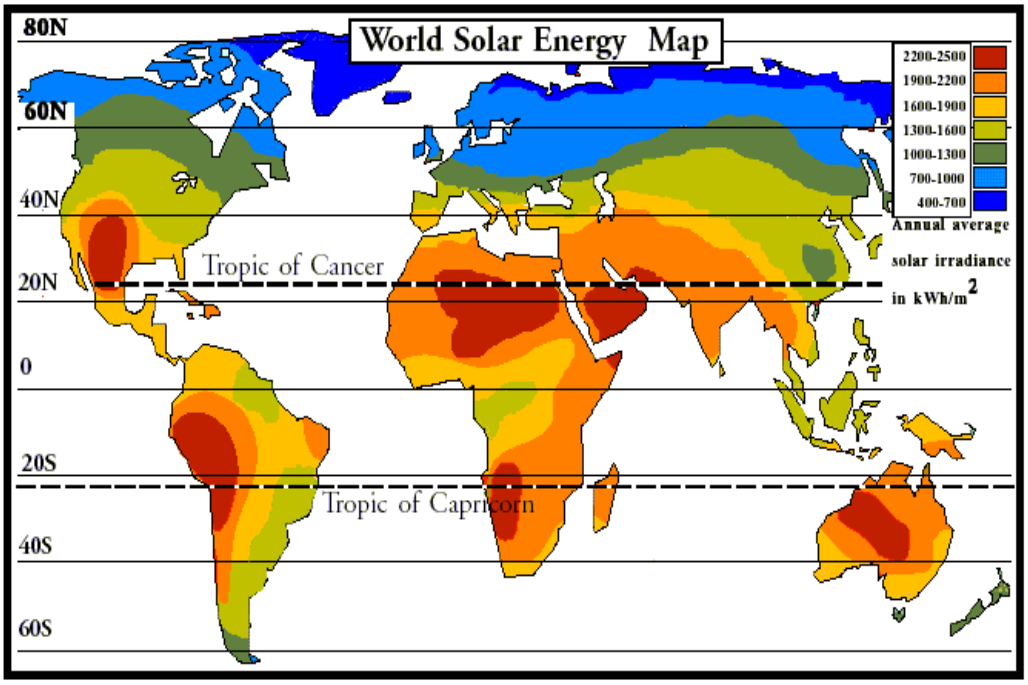

Figure 1.2 Global distribution map of solar energy [11].

1.2 Principle of solar cells

1.2.1 Semiconductors

Depending on the electrical properties, materials are classified in three major categories: metals, insulator and semiconductor. Metals possess very low resistivity (or high conductivity) i.e. ($\rho \sim 10^{-2} - 10^{-8}\ \Omega$m or $\sigma \sim 10^{2}$-$10^{8}\ Sm^{-1}$), while insulators are bad conductors ($\rho \sim 10^{11} - 10^{19}\ \Omega$m or $\sigma \sim 10^{-11}$-$10^{-19}\ Sm^{-1}$), whereas, semiconductors conduct electricity under certain conditions and have resistivity or conductivity somewhere between that of metals and insulators ($\rho \sim 10^{-5} - 10^{6}\ \Omega$ m or $\sigma \sim 10^{5} - 10^{-6}\ Sm^{-1}$) [12]. Metals, insulators and semiconductors are defined on the basis of *energy bands*. Metals have partly full valence band (VB), or it overlaps in energy with the conduction band (CB) (**Figure 1.3**). Metals have availability of empty states in the partially filled band, which helps in excitation or scattering of valence electron into neighbouring state and these electrons transport heat or charge in solids. In case of insulator and semiconductors, VB is completely full and separated from empty CB band by an energy gap, E_g. In both cases the Fermi level (defined as the chemical potential of electrons at absolute zero) E_F, lies in the centre of the band gap. The electrons in the VB are all completely involved in bonding and require an energy equivalent to the band gap to be moved to the nearest available unoccupied level. The energy gap (E_g) in insulators is large (generally >3 eV and does not conduct electricity), while semiconductors possess the E_g in the range of 0.5 to 3eV. The electrons from the VB may gain external energy (> E_g) and move to the CB leaving behind the vacant energy levels or holes in the VB where other valence electrons can move. This way semiconductor conducts electricity due to electrons and holes in CB and the VB respectively [13].

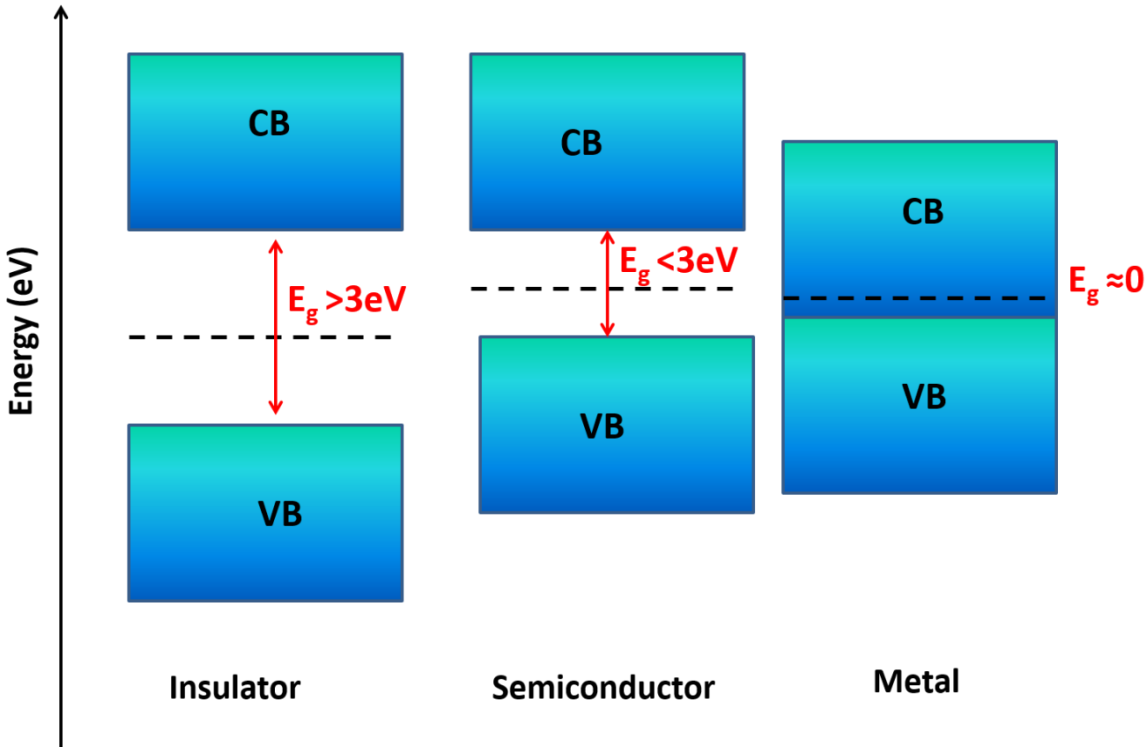

Figure 1.3 Schematic of energy band diagrams of insulators, semiconductors and metals [14].

1.2.2 Working of solar cells

In its simplest form, a solar cell can be described as a semiconductor device which coverts solar energy directly to electric energy through PV effect or as a light absorbing material connected to an external circuit to generate current and voltage.

Solar cells are fabricated by sandwiching the absorber layer i.e. (i-layer) between a n' (n-type semiconductor) layer and 'p' (p-type semiconductor) layer or reverse of that called n-i-p and p-i-n structure respectively as depicted in **Figure 1.4.** The absorber layer or i-layer absorbs most of photons in a solar cell is normally a lightly doped semiconductor with high absorption coefficient. The 'p' layer and 'n' layer are heavily doped p-type and n-type semiconductors respectively. Solar energy contains photons and maximum portion of light is absorbed by i-layer which generates electrons-hole pairs and when solar cell is connected to a metallic wire then electron and hole are transported via electron transport layer (n-layer) and hole transport

layer (p-layer), respectively, generating current. The operation of a solar cell can be separated as 3 main functions:

1) Light absorption and charge generation
2) Charge separation
3) Charge collection

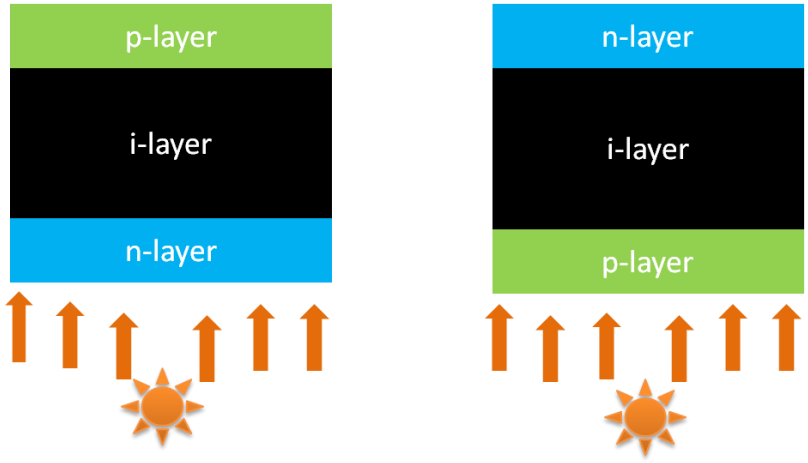

Figure 1.4 Solar cell device structure, n-i-p (left) and p-i-n (right).

Light absorption and charge generation: Charge carriers are generated when a semiconductor is illuminated with a photon having energy greater than its band gap (E_g). Absorption of light results in the photoexcitation of an electron from the VB (ground state) to the CB (excited state). Only photons which possess energy greater than the band gap (E_g) can excite the electron (**Figure 1.5**). When photons, having energy greater than the band gap, falls on semiconductor the electrons are excited to higher energy levels in the CB which rapidly thermalize to the CB minima releasing extra energy in the form of heat. Whereas, photons with energy less than the E_g are either reflected or transmitted through the material. The photoexcitation and thermalization of charge carriers in a semiconductor is schematically depicted in **Figure 1.5.**

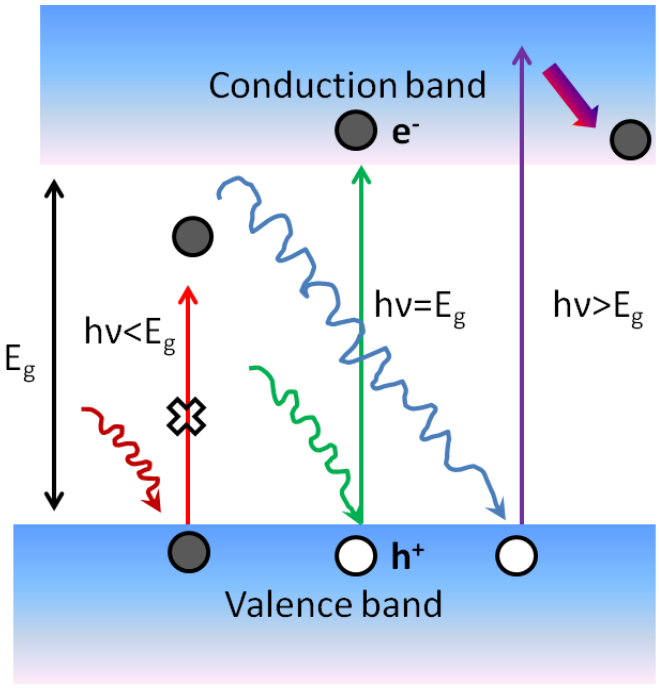

Figure 1.5 Absorption of light (photons) in a semiconductor, based on their energy band gap.

The number of photons absorbed also depends on the incident energy spectrum; the solar spectrum is different depending on the place and time of measurement. Therefore, a fixed reference spectrum is defined, representing the solar spectrum at ground level for mid-latitude regions at a solar zenith angle of 48°. This is a good representation of the overall yearly average for mid-latitudes and is referred to as the Air Mass 1.5 global spectrum (AM1.5G). A total irradiance is also required, and for the same average criteria this is 100mWcm^{-2}. The AM1.5G spectra is shown in **Figure 1.6**.

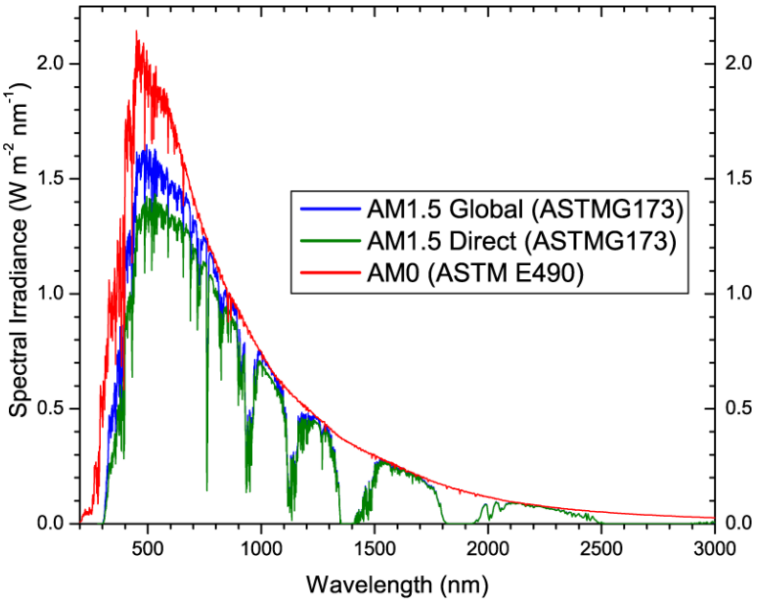

Figure 1.6 Solar irradiance vs. wavelength (λ) for the AM 1.5G solar spectrum incident on the earth's surface [15].

Charge separation: Photo excited electron-hole pair is either bound into an exciton via electrostatic attraction, or the electron and hole act as separate free carriers of negative and positive charges, respectively. The strength and range of this coulombic attraction, or binding energy depend on the specific material. For a given compound, the dielectric constant governs the binding energy of any excitons generated. Generally, exciton has slightly less energy than the unbound electron and hole. For good absorber materials, the binding energy difference ($E_{exci}-\Delta\varepsilon_{e\text{-}h}=-0.012\pm0.009$eV) between the exciton and unbound electron-hole pair energy is very small, and can easily dissociate by thermal energy at room temperature, thereby, generating an electron and hole (free carriers) that freely move independently [16].

Charge collection: In order for charges to be efficiently extracted from PV devices, electron and hole-selective contacts must be placed on the n-type and p-type sides of the p-n junction. This is essential to ensuring that only electrons can be collected at the anode and vice versa [17].

1.2.3 Solar cell performance measurement parameters

The parameters that characterize the performance of solar cells can be determined from the illuminated J-V characteristic as illustrated in **Figure 1.7**. Following are the important parameters:

1. Short circuit current density, J_{sc}
2. Open circuit voltage, V_{oc}
3. Fill factor, FF
4. Power conversion efficiency, PCE

Short current density (J_{sc}): Short-circuit current density (J_{sc}) used to describe the maximum current density that is delivered by a solar cell. J_{sc} of an illuminated solar cell that behaves as the ideal diode is given by

$$J = J_{rec} - J_{gen} - J_{ph} \quad = J_0 \left[\exp\left(\frac{qV}{k_B T}\right) - 1\right] - J_{ph} \qquad (1.4)$$

where, J is the net current density, J_{rec} is recombination current density, J_{gen} is the current density of photogenerated charge carriers, J_{ph} is the photocurrent density, J_o is dark current density, q is the elementary charge, V is the potential difference between contacts, k_B is the Boltzmann's constant and T is the temperature.

Open circuit voltage (V_{oc}): The open-circuit voltage is the voltage at which no current flows through the external circuit. V_{oc} depends on the photo-generated carriers and the quasi-fermi level splitting. V_{oc} can be calculated from **Equation 1.5** assuming that the net current is zero.

$$V_{oc} = nk_B T q^{-1} \ln\left(\frac{J_{sc}}{J_0} + 1\right) \qquad (1.5)$$

where n, k_B and T are ideality factor, Boltzmann constant and temperature respectively.

Fill factor (FF): The fill factor is the ratio between the maximum power generated by a solar cell and the product of V_{oc} with J_{sc}

$$FF = \frac{P_{MPP}}{J_{sc} \times V_{oc}} = \frac{J_{MPP} \times V_{MPP}}{J_{sc} \times V_{oc}} \qquad (1.6)$$

Power conversion efficiency (PCE): The conversion efficiency is calculated as the ratio between the maximal generated power and the incident power. As mentioned above, solar cells are measured under the standard test condition (STC), where the incident light is described by the AM1.5 spectrums and has an irradiance of I_{in} = 1000 W/m^2

$$\eta = \frac{P_{max}}{I_{in}} = \frac{J_{mpp}V_{mpp}}{I_{in}} = \frac{J_{sc}V_{oc}FF}{I_{in}} \quad (1.7)$$

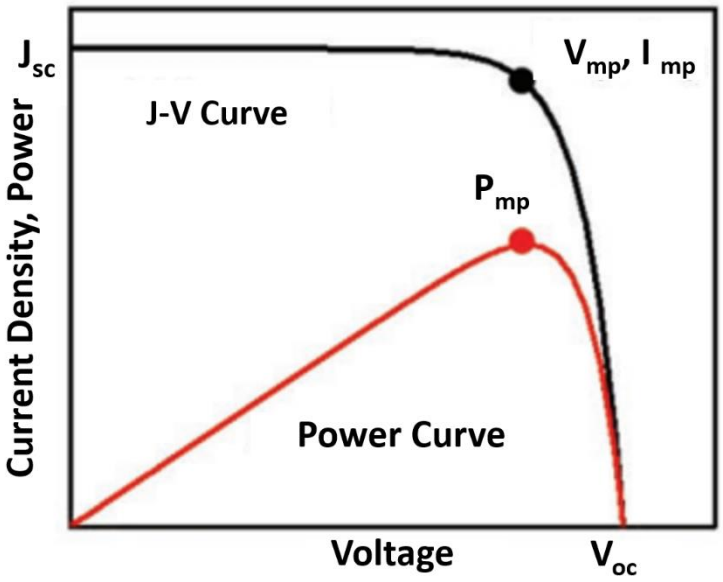

Figure 1.7 Current density-voltage (J-V) curve of typical solar cell.

1.3 Types of solar cells

The classification of solar cells is done based on their generation which is summarized in **Figure 1.8.**

Silicon solar cell: It belongs to first generation solar cell and presently it covers 90% of the PV technology. The large fraction of them are single junction cells based on wafers made from single crystals or polycrystals [18]. Silicon solar cell is based on p-type and n-type silicon. The p-type silicon is doped with group III elements such as boron or gallium that have one less electron in their outer energy level than does silicon which cause the material to be electron deficient and thus an electron vacancy or “hole” is created. On the other hand, n-type silicon is

doped with group V elements, e.g. phosphorus that has one more electron in their outer level than silicon which causes the material to become electron rich. When sunlight strikes a solar cell (p-n junction), holes in the p-doped material diffuse towards the n-doped material and vice versa. The intrinsic electric field in the depletion region, causes the electrons to be pushed to the n-doped side of the junction and holes to be pushed to the p-type side of the junction, effectively causing separation of the charges. Connecting the n-type and p-type layers with a metallic wire, the electrons will travel from the n-type layer to the p-type layer by crossing the depletion zone and then go through the external wire back of the n-type layer, creating a flow of electricity.

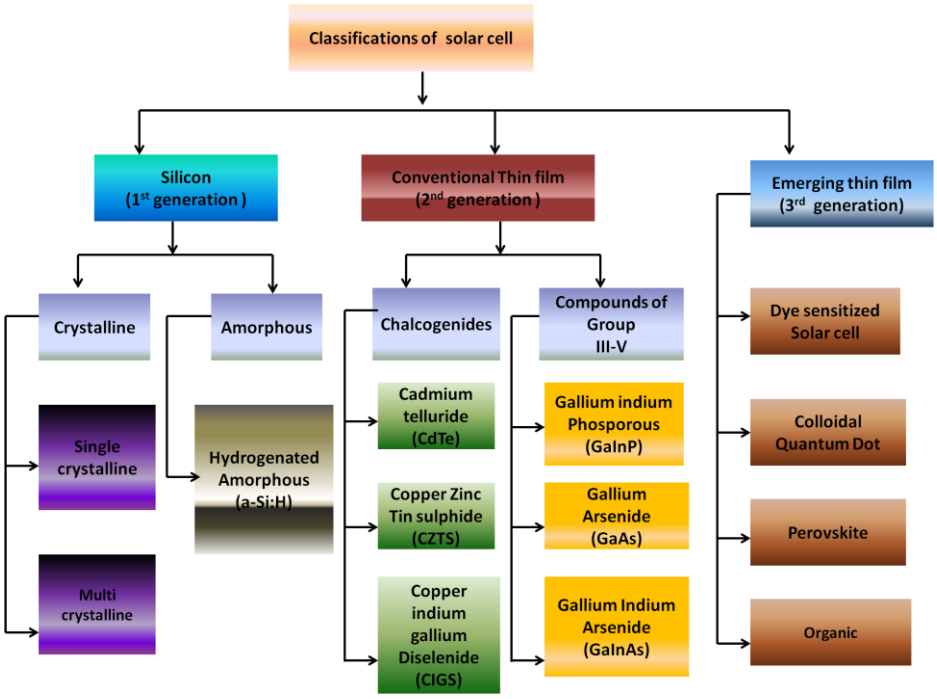

Figure 1.8 Classification of solar cells based on the generation.

Copper Indium gallium diselenide (CIGS): Group I-III-VI compound semiconductors of band gap within the range of 1.01 eV to 1.67 and high absorption coefficients such as Cu(In, Ga)Se_2 (CIGS) and CdTe has shown potential to absorb nearly all incidental solar light, and can be utilized as very thin films (2–3 μm) solar cells [19]. First CIGS thin-film solar cell was

developed in the early 1976s and reported efficiency was 4.5% [20]. Subsequently, CIGS thin-film absorbers, processing, and contacts have improved efficiency from meagre 4.5% to 24.22% in year 2021 for small area thin-film cells [21]. The basic layer construction of a commercial CIGS solar module consists of a substrate carrying a molybdenum back contact, the CIGS absorber layer, a buffer layer, and the highly doped ZnO transparent front contact.

Organic solar cell: Organic solar cells (OSC) are comprised of a junction between two molecular semiconductors (electron donor and an electron acceptor). Since, these are organic molecules therefore electrons are excited between molecular orbitals, with an effective bandgap i.e. difference in energy between the highest occupied molecular orbital (HOMO) and the lowest unoccupied molecular orbital (LUMO). When illuminated photons are absorbed by the polymer, upon photoexcitation charge carriers (electron-hole pair) are generated and subsequently separated at the donor–acceptor interface by exciton dissociation, occurring due to electron transfer from the LUMO of the donor to the LUMO of the acceptor. Charge transport of the hole (from the donor) to the anode and the electron (from the acceptor) to the cathode enables these charge carriers to flow through the external circuit and create electricity as illustrated in **Figure 1.9** [22]. The rapid developments in the field of OSCs has resulted in achieving the PCE of over 18% [23,24].

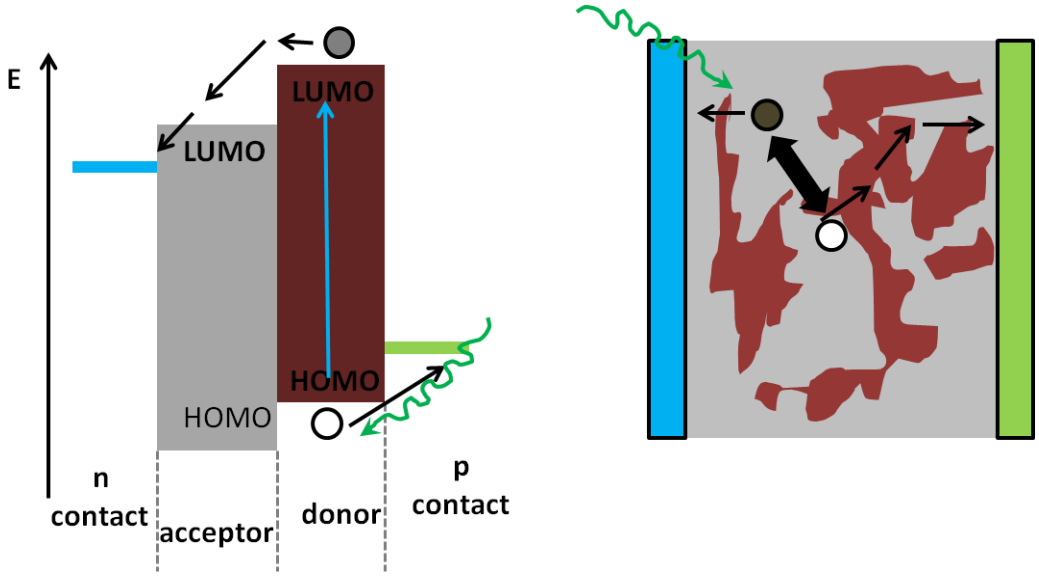

Figure 1.9 The working principle of organic solar cell operation. Left: energy level diagram. Right: Schematic of distributed junction approach between an acceptor material (blue) and a donor material (green). Upon photoexcitation, an exciton is formed in organic region (grey), diffusing until it reaches the interface. It can then split into an electron and a hole, which travel through the respective materials to the contacts [25].

Dye sensitized solar cell: In early 1960, it was discovered that electricity can be generated through illuminated organic dyes in electrochemical cells. Dye sensitized solar cell (DSSC) is composed of a mesoporous semiconductor oxide film electrode, dye sensitizers, electrolytes, counter electrode and transparent conducting substrate. The operational principle of DSSC is illustrated in **Figure 1.10**. When exposed to sunlight, the dye sensitizer gets excited and electron-hole pairs forms in the dye, the electron is rapidly transferred into the n-type semiconductor (normally TiO_2) and the hole into the electrolyte. The electron and hole then travel through the mesoporous semiconductor and electrolyte to the collection electrodes. The built-in field in this case arises from the energetic difference between CB in the semiconductor and the reduction level in the electrolyte; electrons cannot transfer into the electrolyte nor holes to the semiconductor, due to the choice of materials [26].

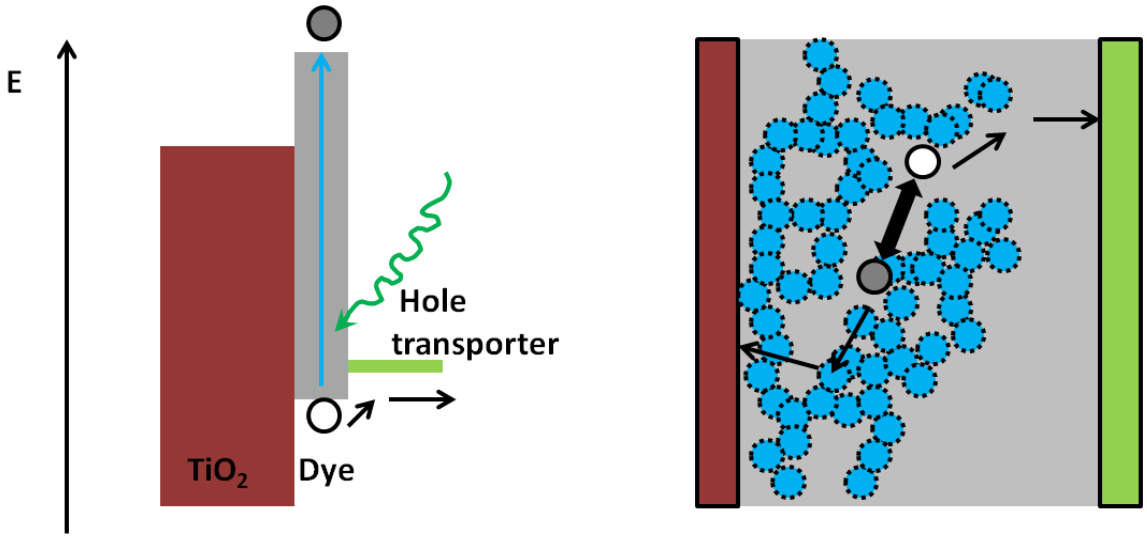

Figure 1.10 The operational principle of DSSC. Left: energy level diagram. Right: schematic of operation. Upon excitation of an exciton in the dye, electrons are rapidly transferred into the TiO_2 and holes to the hole transporter, either an electrolyte or a solid state hole transporter. These materials then transport the charge to the electrodes [26].

1.4 Perovskite solar cells

When it comes to third generation thin film solar cell the first name pops in mind is perovskite solar cell (PSC). Organic inorganic hybrid perovskite (OIHP) gained much popularity because of rapid growth in their efficiency from 3.8% to over 26 % in just 10 years.

The term "perovskite" is applied to any member of the class of materials which have the crystal structure of calcium titanate ($CaTiO_3$). Perovskite materials have a unique property of high charge carrier mobility, ease of electron and hole transport, high absorption coefficients, direct and tunable band gaps and long carrier diffusion lengths. PSCs are mainly based on perovskite material and is represented by the general formula of ABX_3 where, A is an organic cation, which may be either MA^+(methyl ammonium, $CH_3NH_3^+$) or FA^+ (formamidinium, $CH_3(NH_2)_2^+$), or inorganic cations such as cesium (Cs^+) or sometimes mixed cations with an appropriate Cs/MA, Cs/FA, Cs/FA/MA ratio, B is a divalent metal cation such as Pb^{2+} or Sn^{2+},

and X is generally a halide anion such as I^-, Cl^-, Br^-, or F^-[27] **(Figure 1.13a).** In a cubic perovskite structure of ABX_3 composition, two parameters (a_1 and a_2) can be extracted from two Miller planes; a_1 is extracted from (200) plane and is given by two radii of *B* and *X*; and another from (100) plane in which case the a_2 is given by cathetus of the right-angle triangle whose hypotenuse is comprised of two radii of *A* and *X*. The ratio of a_2/a_1, known as Goldschmidt tolerance (GT) factor (*t*), which is given by formula **Equation (1.8)** [28]

$$t_f = \frac{r_A + r_X}{\sqrt{2}(r_B + r_X)} \tag{1.8}$$

where r_A, r_B and r_X are the ionic radii of A, B and X respectively, (t) decides whether a compound will form cubic, tetragonal or rhombohedral perovskite structure [29] for the cubic perovskites, (t) should be close to 1 to form a stable perovskite with no/little structural distortion [30]. The size of cation A is critical for the formation of a close-packed perovskite structure; in particular, cation A must fit into the space composed of four adjacent corner-sharing BX_6 octahedral.

For the first time, Miyasaka and his group in 2009 used $CH_3NH_3PbI_3$ and $CH_3NH_3PbBr_3$ as sensitizers in liquid electrolyte solar cells, achieving power conversion efficiencies of 3.5%. However, later to mitigate the drawback of the instability of liquid electrolyte, solid state hole transporting materials (HTMs) such as 2,2',7,7'-tetrakis (N,N-p-dimethoxy-phenylamino)-9-9'-spirobifluorene (spiro-OMeTAD) was utilized. Since 2012, research into PSC has erupted, and the devices have evolved from a perovskite sensitized, nanostructured configuration utilizing mesoporous TiO_2 to the meso-superstructured solar cell (MSSC) configuration. MSSCs use an insulating material as a mesoporous scaffold, to a simple planar heterojunction all of which have reached reported efficiencies of over 26%. This material has also been shown to operate

efficiently in the “inverted” cell architecture, achieving power conversion efficiencies of up to 15%. The evolution of PSCs overtime is depicted in **Figure 1.11.**

Three different kinds of PSC structures, the mesoporous structure, the conventional p–i–n structure and the inverted i–n–p structure, are shown in **Figure 1.12.** Planar structure consists of conductive oxide substrate, such as fluorine-doped tin oxide (FTO), electron transport layer (ETL) or negative-selective layer (n-type), a perovskite layer (absorber layer), hole transport layer (HTL) or positive-selective contact (p-type) and, a top metal anode such as Au or Ag. In case of inverted structures, the sequence is reversed **Figure 1.12.**

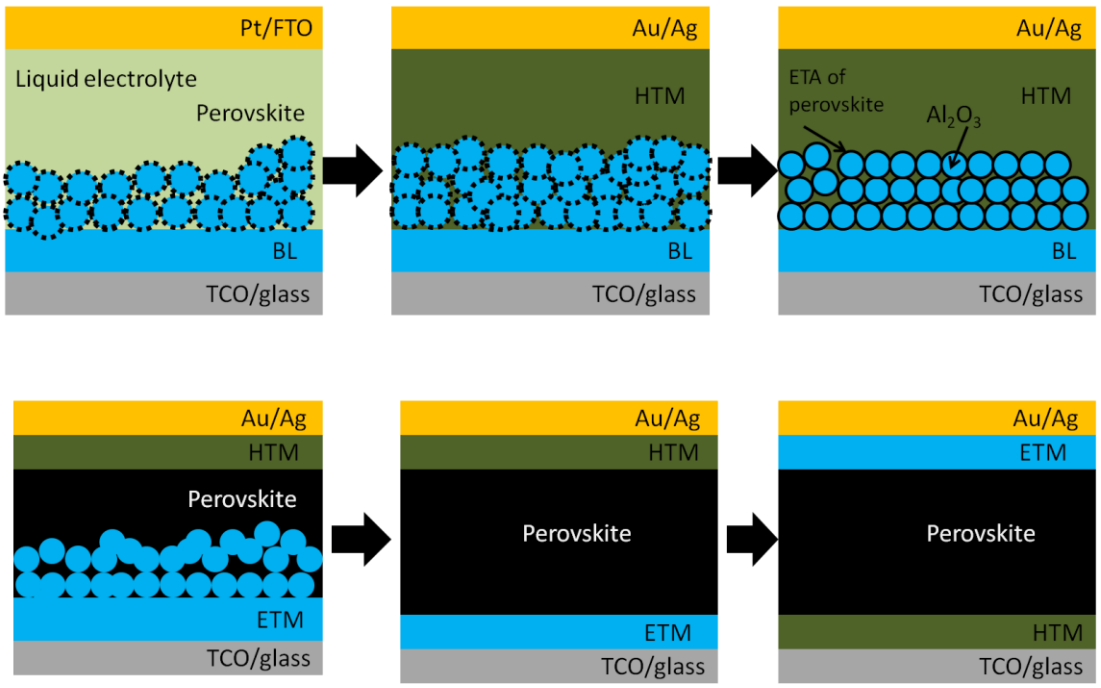

Figure 1.11 Diagram of the evolution of the PSC. From top left to bottom right: Sensitized PSC with liquid electrolyte, solid-state sensitized PSC, MSSC PSC, mesostructured solar cell with thick perovskite capping layer, planar PSC [31].

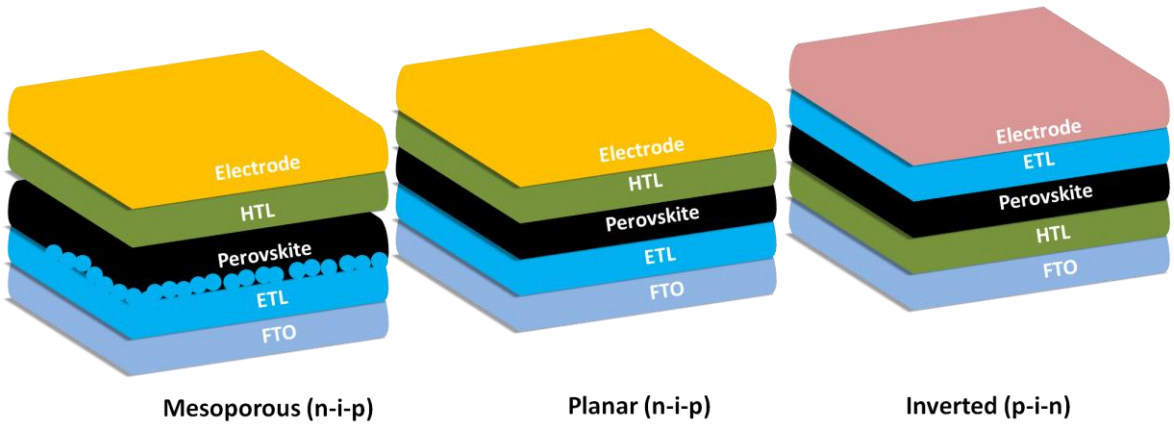

Figure 1.12 Various device architecture of perovskite solar cells.

1.5 Working of Perovskite solar cells

Perovskite materials absorb light, which leads to excitation of an electron from VB to the CB of perovskite and the formation of an electron-hole pair, the equivalent circuit and working diagram of PSC is depicted in **Figures 1.13 b-c**. The charges dissociate willingly because of the low exciton binding energy and their ability to freely move across the device. Due to relatively higher charge mobility and long carrier diffusion lengths, perovskites are efficient in transferring both holes and electrons. Electrons either diffuse to the continuous ETL, or do so through the mesoporous scaffold from the perovskite. Consequently, the electrons are collected at the electrode. Similarly, photogenerated holes diffuse through perovskite to reach HTL and are collected at the metal electrode.

Electron and hole transport layers (also called "blocking" or "charge-selective layers") are vital components of PSCs. ETL blocks the holes and allow electrons to pass to the electrode, and HTL does the opposite, and is achieved via selection of materials having suitable band alignment with perovskites. A good HTL material ought to have its CB or LUMO far above that of perovskite and its VB or HOMO must be just slightly above perovskites VB. The vice-versa holds true for ETL material as shown in **Figure 1.13c.**

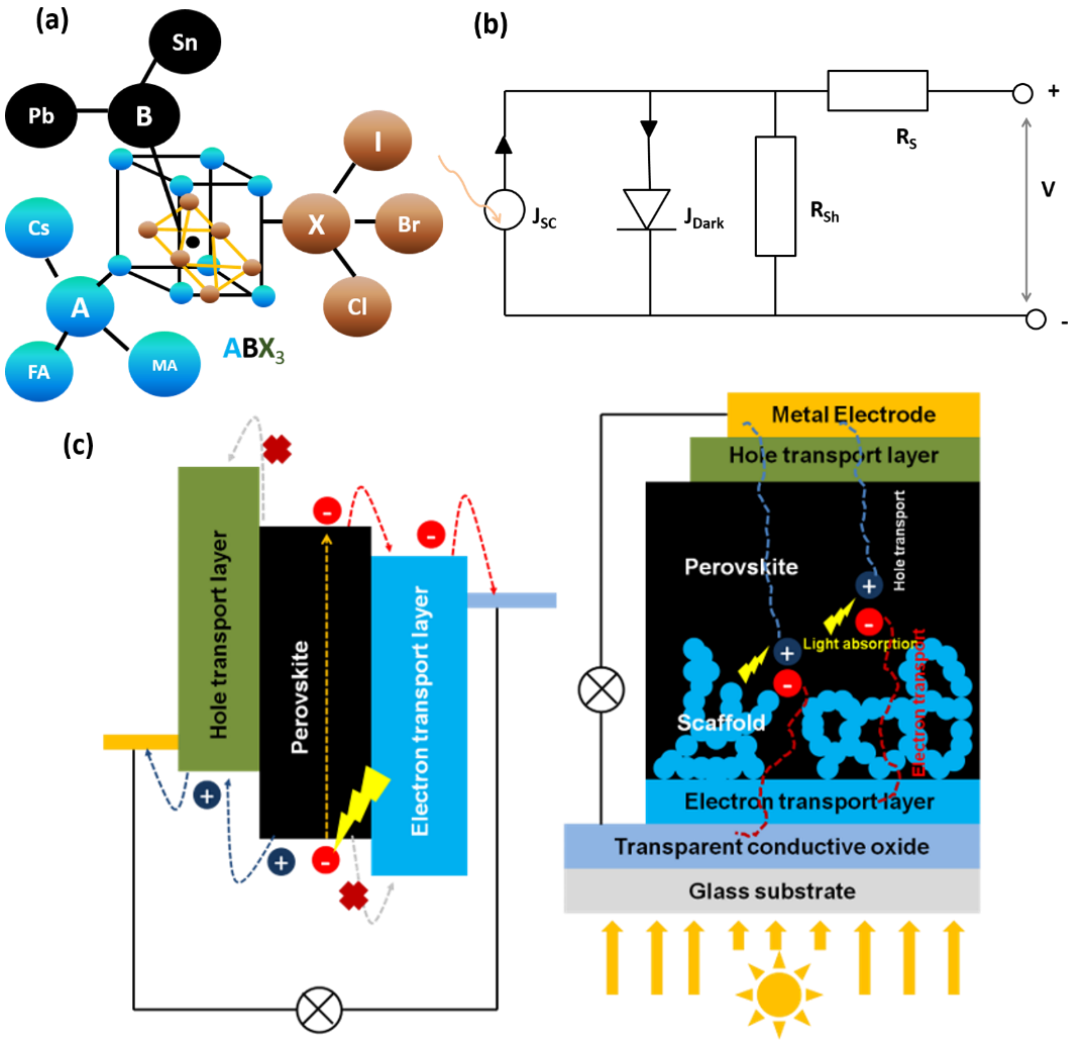

Figure 1.13 Perovskite structure showing the ABX_3 structure, Circuit diagram of PSC and schematic showing the working of solar cells.

1.6 Lead and lead-free perovskite solar cells

Lead-based PSC has achieved such a progressive efficiency from 3.8% to over 26% in less than a decade [32,33]. The exceptional progress made is attributed to its compositionally tunable electronic and optical properties, high absorption coefficient, carrier mobility, longer diffusion length, greater carrier lifetime [34–36], and low-cost solution-based-processing [27]. Although, the lead based PSC received so much attention but toxicity and carcinogenic nature of lead stumbles its commercialization. In recent years, Sn-based PSC has been projected as an

alternate to lead-based perovskite and has accelerates its efficiency from 6% [37] in year 2014 to 12 % in early 2020 [38].

1.7 Issues and challenges

Despite the high efficiency and relatively low cost, poor stability, and faster degradation of device performance of Pb and Sn-based perovskite is the most prominent problem, and major roadblock for the commercialization of PSC. The reason for poor stability of perovskites can be classified into two broad categories: extrinsic and intrinsic. Extrinsic factors are related to the environment such as oxygen and moisture, while the intrinsic factors include thermal instability, hygroscopicity and recombination [39]. The inherent instability of the OIHPs on the exposure of moisture, air or oxygen, thermal and UV illumination contributes to the degradation of the perovskite absorber layer.

1.7.1 Stability of perovskite solar cells

Structural stability

Structural stability of a material is defined by the ability to sustain a certain crystalline phase to be stable at different condition (pressure, temperature) and characterized by the absence of polymorphism [40]. The structural stability of perovskites can be estimated by GT factor which can determine the crystal structure selectivity of a perovskite, expressed by **Equation 1.8** [28].

For the cubic perovskites, ideally (t) should be close to 1. With increasing deviation from the ideal (t=1), the lattice distortion sets in, causing progressively lower symmetry structures become stable. The cubic phase is more probable when the (t) lies between 0.89 to 1, while the lower symmetry phases, such as tetragonal (β phase) or orthorhombic (γ phase), becomes more stable when the t <0.89 [41].

The optoelectronic properties (bandgap, absorption coefficient, carrier mobility and conductivity) also changes with the change in the crystal structure [42]. It is shown that the formamidinium FA($CH_5N_2^+$) based perovskites are more thermally stable than methyl ammonium MA($CH_3NH_3^+$), based perovskites mainly because of the larger size of FA cation (~2.53 Å) when compared to the MA (~ 2.17 Å), which shifts the (t) closer to 1 [43]. GT factor (t) can also be altered by reducing the size of the X site. Introducing inorganic cations such as K^+, Cs^+, Rb^+, at A sites is also shown to enhance the stability of OIHP [44–46].

Effect of moisture and oxygen

Moisture from ambient is unanimously accepted as one of the most important factors contributing to the degradation of Pb and Sn-based perovskites [47]. Organic MA or FA cation, due to their hygroscopic nature, hydrolyses in the presence of moisture [48,49]. Since MA is acidic in nature, gives up a proton to water, forming H_3O^+ by breaking the bond between the organic component at 'A' site and the metal (Pb or Sn) at 'B' site of the perovskite structure. A possible water-mediated decomposition route has been explained by Frost *et al.* [50]. It was proposed that on exposure to moisture, organic iodide forms HI acid which dissolves in water. Although a small amount of water is sufficient to deprotonate the organic part, an excess of water is required to dissolve the HI and CH_3NH_2 by-products for degradation to continue. In the presence of trace amounts of H_2O, partial decomposition of the hybrid perovskite happens until the by-products (either HI saturates the H_2O or CH_3NH_2) reach equilibrium, while in the presence of sufficient water, the perovskite degrades entirely to form metal iodide (PbI_2 or SnI_2). The following reactions are believed to take place during degradation of a Pb-based perovskite in the presence in water [50]:

$$CH_3NH_3PbI_3(s) \leftrightarrow CH_3\ NH_3I\ (aq) + PbI_2\ (s) \quad (1.9)$$

$$CH_3\ NH_3I\ (aq) \leftrightarrow CH_3NH_2\ (aq) + HI\ (aq) \quad (1.10)$$

$$4HI\ (aq) + O_2 \leftrightarrow 2I_2(s) + 2H_2O \quad (1.11)$$

$$2HI\ (aq) \leftrightarrow \quad H_2 \uparrow + I_2\ (s) \quad (1.12)$$

Similarly, $HC(NH_2)_2PbI_3$ decomposes to $HC(NH_2)_2I$ and HI, where $HC(NH_2)_2I$ further decomposes to the volatile sym-triazine and NH_4I [51].

Sn-based perovskite suffers from the rapid oxidation of Sn^{2+} to more stable Sn^{4+} because of lower standard redox potential of +0.15 V for Sn^{2+}/Sn^{4+}, when compared to +1.67 V for Pb^{2+}/Pb^{4+} [52]. Oxidation of Sn^{2+} ion distorts the charge neutrality of the perovskite structure and breaks down into oxides/hydroxides of Sn and MAI or FAI [37] which changes the electronic properties, such as charge mobility, conductivity, diffusion length, and band alignment [53,54]. The oxidation mechanism of Sn^{2+} can be summarized as the following reactions:

$$Sn^{2+} + O_2 \rightarrow SnO_2 + 2h^+ \quad (1.13)$$

$$Sn^{\bullet\bullet} \rightarrow Sn_{Sn}^{x} + 2h^+ \ (Sn_{Sn}^{\bullet\bullet} + 2e^- \rightarrow Sn_{Sn}^{x}) \quad (1.14)$$

It is clear that the oxidation of $Sn^{2+} \rightarrow Sn^{4+}$ results in the creation of an extra pair of hole rendering it p-type [54].

Thermal stability

Thermal instability of PSC is another major hurdle to be pass for their commercialization. The exposure of perovskite layers to heat starts with the annealing process, when it is exposed to higher temperatures (60-200 °C) for times varying from 10 min to 2 h. Annealing temperature plays a critical role in achieving the desired phase of perovskite [55]. $MAPbI_3$ at room

temperature exist in tetragonal phase, (space group *I4cm*). $MAPbI_3$ shows a transition from tetragonal to cubic (or pseudocubic) symmetry when heated above 55 ℃ [56]. $FAPbI_3$ showed phase transition between two polymorphs, that is, a black or alpha (α phase) perovskite with trigonal symmetry (space group *P*3*m*1) forms at higher temperatures, ∼125−165 °C, while a yellow or delta (δ-phase) having a non-perovskite hexagonal symmetry ($P6_3mc$) forming at room temperature [57]. Similar polymorphism was observed in the case of $CsPbI_3$ where α and δ-$CsPbI_3$ phases were reported [58].

Similarly, for Sn-based perovskite methyl ammonium tin iodide ($MASnI_3$), phase transitions occur at ($\sim 2^{o}$ C) and (-165^{o} C) respectively [59]. A cubic structure ($Pm\bar{3}m$) or an alternative pseudocubic (*P4mm*) structure is thermodynamically stable at room temperature, which upon cooling below ~2 °C, converts to tetragonal β-phase (*I4cm* or *I4/mcm*) [51], while on cooling further below -165 °C, orthorhombic γ-phases (*Pbn21* or *Pbnm*) becomes thermodynamically stable [60]. On the other hand, in the case of $FASnI_3$, the phase transition occurs at around -27 °C and -120 °C. It adopts cubic ($Pm\bar{3}m$) structure or pseudocubic α-phase (*Amm2*) at higher temperature, while converts to tetragonal β-phase on cooling (below ~ -27^{o} C) and finally converts to orthorhombic γ-phase at temperature -120 °C [51,61].

PSCs degrades when heated or illuminated in air and oxidizes, the general equation for the oxidation of Pb and Sn-based perovskite can be written as: [62]

$$2ABI_3+O_2 \rightarrow 2AI+BO_2+BI_4 \quad (1.15)$$

UV illumination

PSCs generally utilize compact-TiO_2, sometimes along with mesoporous-TiO_2 layers, as ETL. TiO_2 is a popular photocatalyst which can catalyze degradation of perovskite in the presence of UV. The degradation due to UV is explained by the fact that TiO_2, being an n-type

semiconductor, have many oxygen vacancies located at the surface. These deep electron-donating sites combine with oxygen, which is adsorbed at the oxygen vacancy sites at the surfaces. Upon exposure to UV radiation, an electron-hole pair is created in TiO_2. The hole in the VB, combines with the electron at the oxygen surface site resulting in the desorption of O_2 and the creation of an oxygen vacancies which act as trap states for photo-induced electrons generated in the perovskite layer. These trapped electrons recombine with holes from the HTL. The creation of the active traps sites is responsible for the photocurrent degradation in the solar cell. The earlier reports has demonstrated that upon the illumination ($1mWcm^{-2}$) of lead halide perovskites increases the halide vacancy concentration, resulting in increased ionic conductivity which leads to the ion migration in PSCs [63].

Poor film morphology

Perovskite film morphology and crystallinity are found to be crucial factors in fabricating highly efficient and stable solar cell. The rapid and uncontrolled crystallization of Pb and Sn-based perovskite result in films with dendritic microstructure, pin holes and non-uniform coverage [64]. These structural defects are also the active sites for charge recombination, charge trapping and leakage [65] which further affects the overall performance of the solar cell [66]. As a result, the perovskites degrade rapidly which is indicated by its colour change from black brown and yellow to almost transparent in the presence of oxygen and moisture [67, 68].

Charge recombination

Charge recombination characterizes the loss of useful carriers by electron-hole recombination process, any electron, excited to the CB by absorption of radiation is in a metastable state and it tries to stabilize to a lower energy position in the VB. Dropping of excited electrons from the CB to VB, to occupy empty state in VB, result in loss of the current and efficiency of the cell. Recombination is affected by several factors such as energy levels of charge extraction materials, bulk and interface defects, charge mobility of perovskite and/or contact materials,

and charge diffusion length [69]. Three types of Recombination namely: radiative, non-radiative (Shockley-Read Hall) and auger recombination are very common [70]. Radiative recombination occurs when an electron from the CB directly combines with a hole in the VB releasing photons having energy comparable to the bandgap. On the other hand, non-radiative recombination (also known as Shockley−Read−Hall) is a non-fundamental decay channel mediated by defects [52]. While in the case of an Auger recombination, an electron and a hole combine and the energy released results in ejection of a third carrier which generally thermalizes down to the conduction band edge.

Hysteresis

PSC shows hysteresis behaviour in J-V curve *i.e.* higher current in reverse scan (positive to negative scan or from short circuit to open circuit) than the forward scan (negative to positive or from open circuit to short circuit) which arises due to the difference in J–V curve from reverse scan ($V_{oc} \rightarrow J_{sc}$) and forward scan ($J_{sc} \rightarrow V_{oc}$) and causes the difficulty in evaluation of the real performance of the devices. Snaith *et al.* [71] and Xiao *et al.* [72] were the first to study the J−V hysteresis behaviour in the mesoporous and planar PSCs respectively. Hysteresis is generally quantified as hysteresis index (HI) which is defined as:

$$\mathrm{HI} = \frac{\mathrm{PCE_{rev}}}{\mathrm{PCE_{for}}} - 1 \qquad (1.16)$$

where PCE_{rev} and PCE_{for} are the PCE obtained in reverse and forward scan, respectively [73]. The slow ion migration of cations and anions [74,75] ferroelectric polarization [76] charge trapping and capacitive effects, are identified as the possible major causes for the hysteresis in J-V curve [77]. Moreover, there are other phenomenon which has been claimed to be associated with the J−V hysteresis which include giant dielectric constant [72,78] unbalance between hole and electron mobility [79] ferroelectricity [77] and charge trapping [80]. However, the exact reason and mechanism behind the hysteresis is still matter of debate.

1.7.2 Steps for stability improvement

Additive and Solvent engineering

The morphology of perovskite film can be tuned by controlling nucleation and crystal growth, for this purpose additive and solvent engineering is a very viable strategy. Various additives were utilized to enhance the stability and performance of PSC. Li *et al*. [81] passivated the $CH_3NH_3PbI_3$ perovskite grains by adding phosphonic acid ammonium additive. The crosslink between additive and neighbouring grains in the perovskite structure, through strong hydrogen bonding of the $–PO(OH)_2$ and $–NH_3^+$ terminal groups to the perovskite surface improved the performance and also provides high immunity to PSC towards moisture. Similarly, addition of 4-tert-butylpyridine (tBP), the tertiary butyl group in tBP is highly hydrophobic, leading to the formation a hydrophobic layer on the surface of $CH_3NH_3PbI_3$ enhance the performance and stability.

Solvent engineering *i.e*. dripping of an anti-solvent such as chlorobenzene (CB), toluene and diethyl ether (DE) during spin coating has also been reported to help in improving the quality of the films and allow good coverage of the substrate [82]. Coordinating solvents such as dimethyl sulfoxide (DMSO) and dimethyl formamide (DMF) addition of SnF_2 (reducing agent) and dripping of toluene and CB (anti-solvent) has been successfully utilized to slow down the crystallization resulting in compact films with desirable morphology [68].

Compositional Engineering

Composition engineering which involves mixing of A cations (MA^+, FA^+, Cs^+), B cations (Sn^+, Pb^+) and X anions (I^-, Br^-, Cl^-) has been projected as an efficient way to tune the properties of perovskites and enhance the performance of PSCs. The mixing of the A cations is the most commonly employed methods in compositional engineering [83,84]. Saliba *et al.* [85] used triple cations, Cs, MA, and FA, to achieve highly stable and efficient PSCs. The triple cation based perovskite device gives stabilized PCE exceeding 21% and ~18% following 250 hours

under operational conditions. Gao *et al.* [86] mixed small amount of Cs in $FASnI_3$ based PSC and exceeded the PCE from 3.73 to 6.08% with $FASnI_3$ and $Cs_{0.08}FA_{0.92}SnI_3$ and much enhanced device stability against illumination, heating, and air. It is shown that that Cs with small size could insert into the lattice, leading to the volume shrink of $FASnI_3$ crystal cell, and also beneficial to lowers the free energy of the perovskite, resulting in improving its structural stability.

Incorporation of bigger cations

Several reports suggest that replacing of the hydrophilic cations with hydrophobic long alkyl chain cations such as such as phenyl ethyl ammonium (PEA^+) [87] ethylene diammonium (EDA^{2+}) [88] guanidinium (GA^+) [89] and butyl ammonium (BA^+) [90] can enhance the stability of PSC. Addition of larger cation not only slow down the crystallization but also disrupts the 3D structure into a layered quasi-2D structure, it expands the unit cell larger and the lattice parameters gradually increase, converting into layered structure which attributes in restricting the oxygen and water diffusion, improving the stability of the cell, albeit, at the expense of the device performance [91]. Heavier cation guanidinium (GA^+) has been explored in varied proportions into the formamidinium (FA^+) $FASnI_3$, in the presence of 1% $EDAI_2$ as an additive by Jokar *et al.* [89] and reported the PCE of 9.6% (J_{sc}=21.2mAcm^{-2}, V_{oc}=0.619 V, FF=0.729) and demonstrated stability for 6 days in air without encapsulation.

Inorganic ETL and HTL material

Inorganic metal oxides such as zinc oxide (ZnO), [92] stannic oxide (SnO_2), [93] as well as metal sulfides such as zinc sulfide (ZnS), [94] and cadmium sulfide (CdS) [95] could be used as an alternative ETL material, has been projected as the possible alternative to TiO_2 due to its similar band gap (3.2eV), much higher electron mobility than TiO_2 which enhance electron extraction, and electron transportation in the cell [96]. Similarly, the inorganic HTMs such as nickel oxide (NiO), [97] cuprous oxide (Cu_2O), cupric oxide (CuO), [98] cuprous iodide (CuI),

[99] copper indium disulfide ($CuInS_2$), [100] copper zinc tin sulfide (CZTS), [101] copper thiocyanate (CuSCN), [102] carbon and graphene oxide-based (GO) HTMs [103,104] are accepted as HTLs. Inorganic HTMs exhibit better chemical stability, excellent transmittance, wide band gap, and favourable work function (≈−4.8 eV) and energy level alignment with the perovskite, which facilitates the efficient hole collection [105–107].

Inverted device structure

It has been observed that the planar (n-i-p) structure shows greater J–V hysteresis, due to charge accumulation at the interfaces, and therefore hysteresis arises on the interface ETL/perovskite [71]. Hysteresis can be minimized by adopting inverted structure, where PCBM/C_{60} is used as a charge transport layer, it distributes uniformly over the film and diffuse into defects and grain boundaries and enlarge the contact area which facilitates the efficient charge extraction, at the same time, passivates the defects and holds the mobile ions to form radicals which suppresses the hysteresis [108].

Device encapsulation

Device encapsulation has been demonstrated to improve device stability under simulated sunlight and ambient air [109]. A large range of materials have been explored for device encapsulation including Teflon® [110] Al_2O_3 [111] poly(methylmethacrylate) [112] Poly[2-methoxy-5-(3,7-dimethyloctyloxy)-1,4-phenylenevinylene] (MDMO-PPV) [113] SiOx [114] SiOx/ SiNx [115] ethylene vinyl acetate (EVA) [116] ethylene-methyl acrylate (EMA) [117] polyvinyl butyral (PVB) [118] polymer cyclized perfluoropolymer [119] tantalum–silicon–oxygen (Ta–Si–O) and tantalum–silicon–nitrogen (Ta–Si–N) [120].

1.8 Motivation

The energy crisis due to exhaustion of resources and negative impact of burning of fossil-fuels demands to rely more or more on renewable sources of energy such as solar, wind, biomass,

and geothermal. One of the most promising alternatives is PVs, which generate electricity directly from sunlight a natural energy source that never runs out. There has been tremendous growth in the PV market, and the energy generation cost of PVs is now approaching a level comparable to other energy resources. To further reduce cost, the PCE of PV technology must be increased. Within a decade, the emerging PSCs, have attracted a lot of attention because of its impressive optoelectronic properties which raised the PCE from 3.1% to over 26% making it one of the most efficient thin-film solar cells [121]. The efficiency graph by NREL (**Figure 1.14)** shows exponentially rise in PCE, which assures that PSC is one of the most promising future candidates for low-cost solar power. However, the stability of PSCs remains a stumbling block for its large-scale implementation.

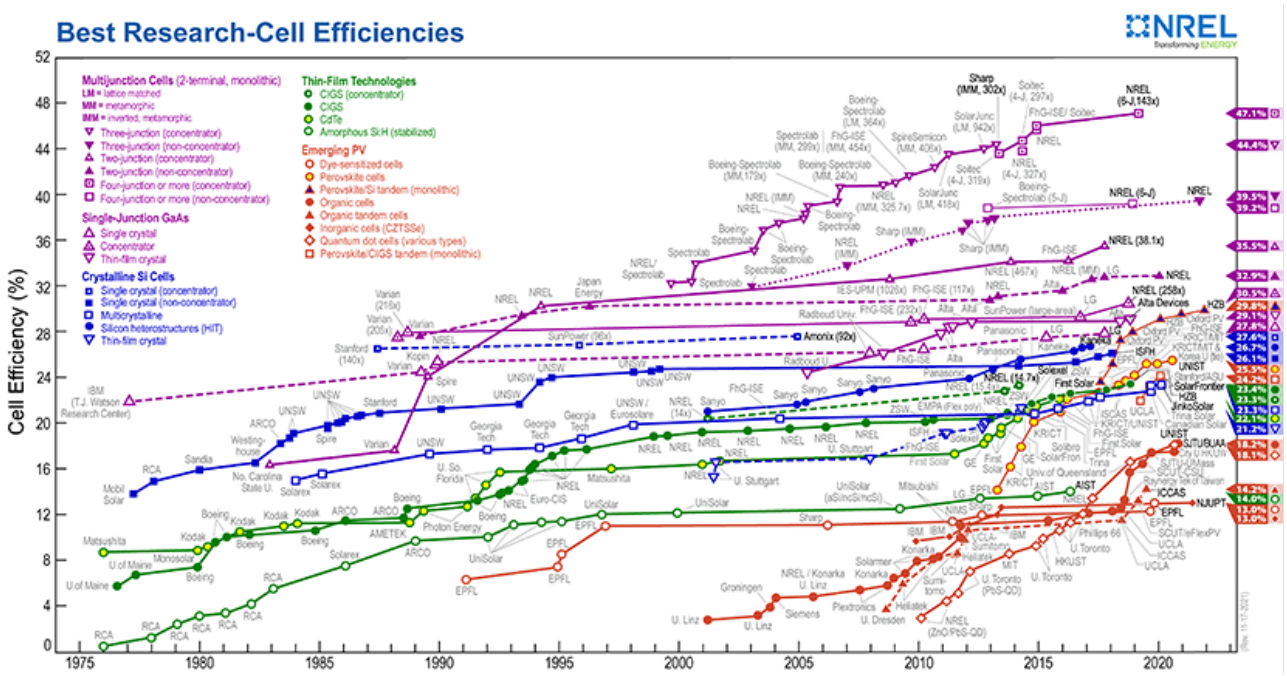

Figure 1.14 Graph showing the trend of efficiency of various types of solar cells during the past four decades. Adapted from National renewable energy laboratory (NREL) [121].

1.9 Scope and Objectives

The scope of the present work is to develop different strategies to improve the stability of organic-inorganic lead and lead-free hybrid perovskite (OIHP) absorber layer and to study the various stability such as structural, thermal and stability in the ambient air, humid and heat condition which can be adopted by considering following steps:

1. Synthesis of Pb and Sn-based perovskite absorber layer with different additives, and antisolvent to study the evolution of microstructure.
2. Study the stability of perovskite layer in ambient air (RH 60-75%) and at temperature (65-85ºC).
3. To optimize the deposition parameter such as annealing time and temperature, and condition of synthesis with different electron and hole transport layer.

To this end, the primary objectives of this work are:

1. To synthesize the perovskite absorber layer with good in ambient and thermal stability.
2. To study different factors affecting the film microstructure of perovskite film such as additives and solvent engineering, annealing temperature and parameters.
3. To study the role of ETL on the stability of perovskite absorber layer deposited.
4. To develop an efficient and stable device with different perovskite absorbers (mixed anion and mixed cation) and study their stability.

1.10 Organisation of Thesis

This thesis focuses on improving the stability of solution processed OIHP absorber layer. The thesis is divided into six chapters.

Chapter I presents a brief overview of the importance, working principle and evolution of solar cell technology. The chapter briefly describes different types of thin-film solar cells,

including PSCs. In the later part of the chapter, the need and motivation of the current investigation, significant challenges and objectives of the dissertation are described.

Chapter II methodology which introduces material, processing methods and characterization/ analytical techniques utilized during the dissertation work. Different perovskite system including mixed cation and anion and fabrication of their complete device is mentioned in details.

Chapter III deals the various parameters affecting the film microstructure during the film fabrication such as solvents, additives, annealing temperature and condition of annealing in detail. The morphological study of Pb and Sn-based perovskite is done by adopting different additives, co-solvent, and different annealing temperature and condition.

Chapter IV explores the effect of wettability and roughness on the microstructure and the degradation of $FAMAPbI_3$ perovskite layer deposited over TiO_2, SnO_2 and TiO_2-SnO_2 bilayers. The role of ETLs on the device performance is studied by fabricating PSC on different ETL namely TiO_2, SnO_2 and TiO_2-SnO_2.

Chapter V describes the structural and thermal stability of FA-MA-Cs containing triple cation perovskite absorber layer. The role of triple cation on the performance of PSC is discussed. The thermal stability of PSC with triple cation is monitored for 1000 hours.

Chapter VI presents the overall summary and conclusions. Along with the conclusions, future prospects in this area are also discussed.